



High-performance flexible transparent conductive thin films on PET substrates with a CuM/AZO structure

Yajie Li¹ · Muying Wu² · Yongtao Sun¹ · Shihui Yu³

Received: 21 April 2019 / Accepted: 12 June 2019 / Published online: 15 June 2019
© Springer Science+Business Media, LLC, part of Springer Nature 2019

Abstract

Hybrid transparent conductive thin films (TCFs) with a bilayer structure composed of aluminum-doped zinc oxide (AZO) and Cu micro-mesh (CuM) are prepared on polyethylene terephthalate (PET) substrates. The AZO layers are deposited by RF magnetron sputtering at room temperature. The CuM is fabricated by UV-lithography and DC magnetron sputtering. The optical properties and conductivity can be modified by the thickness of CuM, and the conduction mechanism involving metal Cu–AZO carrier injection is proposed. The flexible CuM/AZO composite thin films exhibit outstanding optoelectronic performance, with the best figure of merit ≈ 1247 (at average optical transmittance of 85.8%, sheet resistance of 1.9 Ω/sq . and resistivity of $1.89 \times 10^{-4} \Omega\cdot\text{cm}$), as well as excellent mechanical flexibility. The resulting hybrid TCFs with CuM/AZO composite structure show potential applications in flexible electronics, organic light emitting diodes and photovoltaic devices.

1 Introduction

Indium tin oxide (ITO) thin films are highly degenerated, wide-gap semiconductors and have high transparency in the visible region and low resistivity [1, 2]. Because of their unique properties, ITO thin films dominate the market in high-end optoelectronics, such as flat panel displays, organic light emitting diodes, plasma display panels and solar cells [3–6]. However, ITO suffers from high processing temperature and brittleness and is composed of the expensive rare element indium [7, 8], which mean that alternative transparent conducting oxides (TCOs) must be found. ZnO thin film is one of the most popular alternatives used for TCOs due to its n-type conductivity and wide band gap (3.37 eV) [9, 10]. What is worth mentioning, its electrical conductivity

can be enhanced by ion doping such as aluminium (Al) [11, 12], gallium (Ga) [13, 14], indium (In) [15], tin (Sn) [16], niobium (Nb) [17], molybdenum (Mo) [18], and phosphorus (P) [19, 20]. Among them, aluminum-doped zinc oxide (AZO) is one of the most promising alternatives, which is non-toxic, low cost and environmentally friendly [11, 21].

In recent years, along with the rapid development of the flexible electronics, there has been considerable interest in the use of AZO thin films deposited on flexible polymer substrates [22, 23]. However, AZO thin films are required grown at a substrate temperature higher than 250 °C and annealed at a temperature higher than 300 °C in order to meet the desirable optoelectronic properties [12, 21], which are undesirable due to the low thermal resistance of the polymer substrates. To solve the problem, AZO/metal/AZO tri-layer thin films prepared on flexible polymer substrates have been widely investigated by many researchers [24–28], which have lower resistivity than that of the flexible AZO single layer films at the same optical transmittance. Unfortunately, the brittle nature of tri-layer films limits their applications in flexible electronics, because the films crack easily and delaminate when the substrate is bent, which results in the deterioration of both their optical and electrical properties [29]. Therefore, it becomes very hard to obtain the high-quality flexible transparent conducting thin films by using the multilayer structure.

Copper metal mesh (CuM) has intriguing mechanical, optically transparent and conductive properties [30].

✉ Yongtao Sun
sunyongtao100@163.com

✉ Shihui Yu
ysh728@126.com

¹ Department of Mechanics and Tianjin Key Laboratory of Nonlinear Dynamics and Control, Tianjin University, Tianjin 300350, China

² School of Electronic Engineering and Intelligentization, Dongguan University of Technology, Dongguan 523808, Guangdong, China

³ School of Microelectronics, Tianjin University, Tianjin 300072, People's Republic of China

Unfortunately, the adhesion to polymer substrates is very weak and the CuM prepared on polymer substrates easily drops off, resulting in the complete failure of CuM based transparent conducting thin films [31]. In previous studies, the copper layers exhibited excellent adhesion to the oxygen layer at the deposition thickness of above 100 nm [32]. Thus, the high-performance flexible transparent conducting thin films are expected to be prepared by combining the CuM and flexible AZO thin films. In addition, flexible polymers are usually considered as substrates because of their transparency, transportability, low weight and high resistance to impact damage. Many types of polymer substrates, such as polyethylene naphthalate (PEN), polyethylene terephthalate (PET), BOPET, polyethersulfone (PES), polyimide, polycarbonate and so on, are available [33–36]. Among them, PET has been widely used as substrates in flexible electronics because of its excellent optical and mechanical properties, such as high transparency (> 95%), high Young's modulus (14.1 GPa) and high tensile strength (160 N/mm²) [37, 38].

In this paper, we demonstrate a method of fabricating mesoscale CuM structures. The CuM are prepared on the flexible AZO thin films which were fabricated by magnetron sputtering. The optical, electrical and flexible properties of the CuM/AZO composite thin films fabricated on PET substrates are investigated. The typical composite thin films exhibit a transmittance of 85.8%, a sheet resistance of 1.9 Ω /sq. and a resistivity of $1.89 \times 10^{-4} \Omega \cdot \text{cm}$, as well as good flexibility.

2 Experimental procedure

2.1 Deposition of AZO thin films

AZO thin films were deposited on PET substrates by RF magnetron sputtering via using the AZO ceramic target, and the composition of the AZO is ZnO:Al₂O₃ = 98:3 (wt%). The PET substrates were cleaned with a cotton swab and the liquid detergent, rinsed thoroughly with another cotton swab and the deionized water, and then further cleaned by ultrasonication in isopropanol and deionized water for 10 min before being dried with N₂. The sputtering distance between the target and the substrate was 5.5 cm. High purity argon and oxygen were used as the sputtering gases. The sputtering pressure was 1.0 Pa. The Ar/O₂ ratio was 8:1. The substrate temperature was room temperature and the sputtering power was 100 W. The thicknesses of AZO thin films were controlled at about 200 nm.

2.2 Photolithography-based fabrication of the CuM

The AZ P4620 (Clariant, Switzerland) photoresist was spin-coated on AZO/PET at 2000 rpm for 30 s and the coating

thickness was about 1.2 μm . Then, the coatings were baked on a hotplate at 100 °C for 3 min. Thereafter, the photoresist coatings were exposed using an OAI 100 mask aligner and developed in a developer for 20 s. Then, the patterned photoresist layers (photoresist template) were hardened baking at 120 °C for 2 min. Next, the conductive metal of Cu was prepared onto the photoresist template by DC magnetron sputtering to form uniform Cu mesh seed layer in the micro-trenches on the AZO/PET (Here, the sputtering distance between the target and substrate was 5.5 cm, the high purity argon was used as the sputtering gas, the sputtering pressure was 1.0 Pa, the substrate temperature was room temperature and the sputtering power was 50 W). Finally, the lift-off technique was used to produce the pure Cu metallic meshes. The thicknesses of CuM were set as 300 and 800 nm, respectively.

2.3 Characterization and measurements

The thickness of the thin films was measured by Alpha-Step D-100 profilometer (KLA-Tencor, California, USA). The structure was characterized by FangYuan DX-2700 X-ray diffraction (XRD) system (Dandong, China). The optical photographs and micrographs were obtained using the mobile phone (iPhone 6s plus) and the optical microscope. The surface micrograph was observed by the field emission scanning electron micrograph (FE-SEM, JEOL JSM-6701 F). Optical transmittance spectra and absorption spectra were obtained on an ultraviolet–visible–near infrared (UV–Vis) spectrophotometer (Varian Cary 5000) in the wavelength range 350–800 nm. The electrical properties (electrical resistivity, Hall mobility, carrier concentration, and sheet resistance) were measured by the Hall measurements in van der Pauw configuration (Ecopia HMS 3000 Hall System, Republic of Korea) and the four-point probe instrument (SX1934, SuZhou, PR China). The flexibility tests were performed using a homemade instrument that had a bending radius of ~ 2 mm and a bending speed of one cycle per second. All of the measurements were carried out at room temperature.

3 Results and discussions

The fabrication procedure of the CuM/AZO composite thin films on the PET substrates can be seen in the schematic of Fig. 1a, as described in the Experimental section. First, AZO thin films are deposited on the PET substrates by RF magnetron sputtering (step 1). Then, a layer of photoresist is deposited on the surface of AZO layer (step 2). In step 3, the designed metallic mesh patterns are patterned by UV-lithography. In step 4, the patterned photoresist layer (photoresist template) is hardened baking at 120 °C

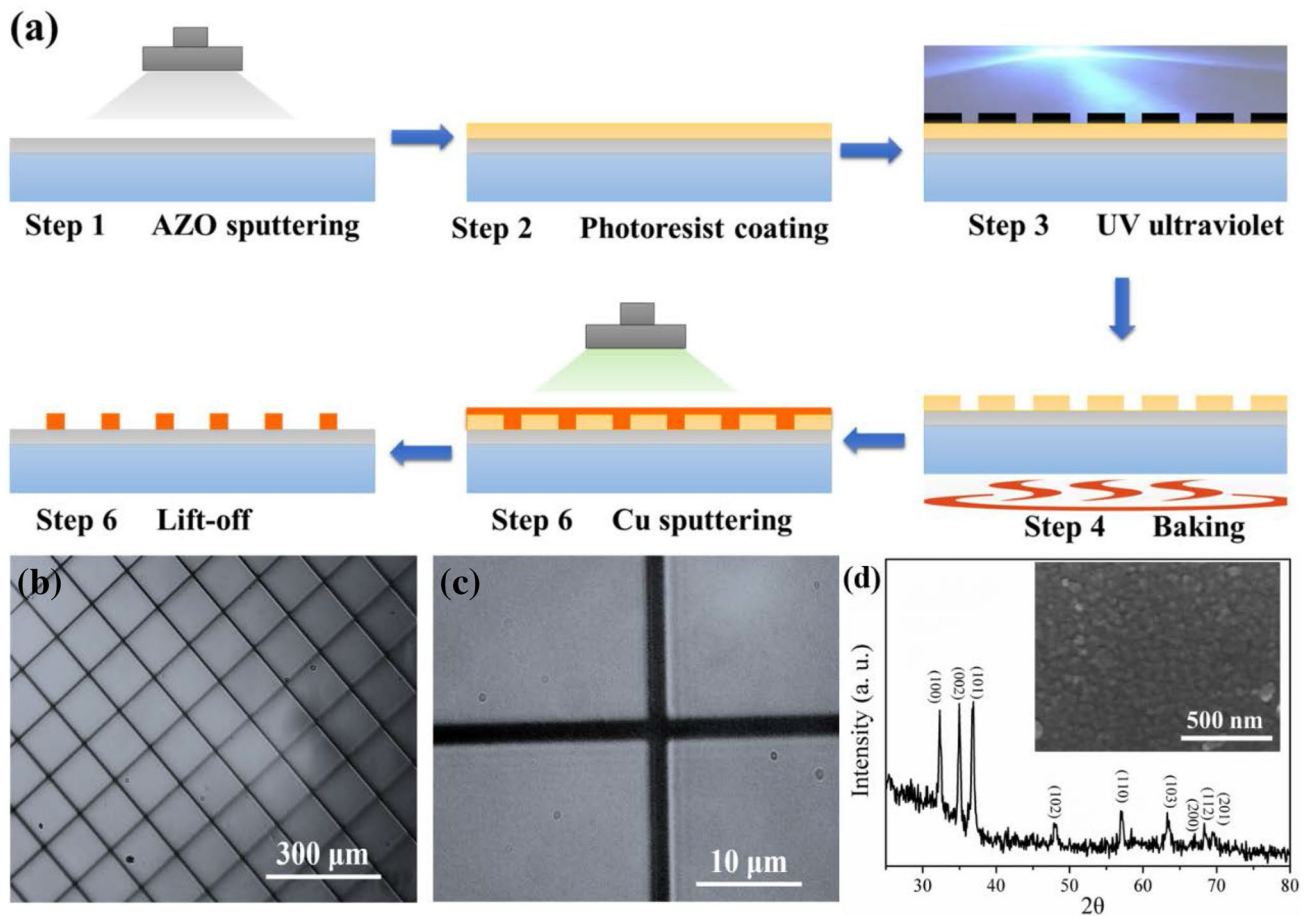


Fig. 1 **a** Fabrication procedure of the CuM/AZO composite thin films on the PET substrates; **b, c** Optical micrographs of the CuM/AZO composite thin films; **d** X-ray diffraction data of AZO thin films, of which the inset is the FE-SEM surface morphology of the AZO thin films

for 10 min. In step 5, the conductive metal of Cu (300, 800 nm) are deposited onto the photoresist template to form uniform Cu layer in the micro-trenches on the AZO layer. Finally, the lift-off technique is used to produce the pure Cu metallic mesh. Figures 1b and c show the optical micrographs of the CuM/AZO composite thin films. It can be seen that metallic Cu meshes keep well their shapes and patterns, in which the width of the Cu mesh is about 2.5 μm and the distance between two Cu meshes is about 150 μm . The large space between the Cu metallic meshes is benefit to optical transmission, resulting in the favorable visual comfortableness. Figure 1d shows the X-ray diffraction pattern of AZO thin films prepared on PET substrate. The AZO thin films are found to be polycrystalline with (100), (002), (101), (102), (110), (103), (200), (112) and (201) planes. The hexagonal wurtzite phase of the synthesized materials are confirmed by comparing with JCPDS data. Inset of Fig. 1d shows the FE-SEM surface morphology of the AZO thin films. It can be observed that the surface is homogeneous and there are no cracks or peeling off. The good physical properties of the AZO

thin films are the basic requirement for the fabrication of hybrid transparent conductive thin films.

The fabrication process in this paper allows easy control and variation of the CuM thickness while not considerably altering the lateral dimension of the CuM, thus providing a feasible method for improving the electrical conductivity without sacrificing their transmittance. Inset of Fig. 2 shows the visual effect of optical transparency for polished CuM/AZO composite thin films on the PET substrates. Figure 2 shows the optical transmittances of the single-layer AZO thin films and the CuM/AZO composite thin films with Cu thicknesses of 300 and 800 nm in the 350–800 nm wavelength range. The average optical transmittance (T_{av}) can be computed as follows [39]:

$$T_{av} = \frac{\int V(\lambda)T(\lambda)d\lambda}{\int V(\lambda)d\lambda} \quad (1)$$

where $T(\lambda)$ is the transmittance and $V(\lambda)$ is the photopic luminous efficiency function defining the standard observer for photometry [39]. According to Eq. (1), the optical

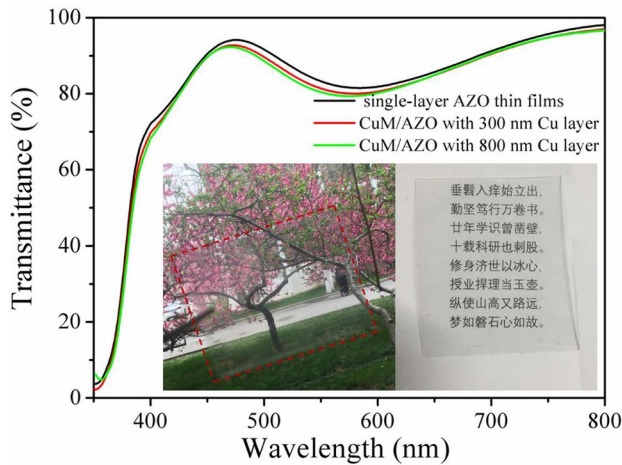


Fig. 2 Optical transmittance of the single-layer AZO thin films and the CuM/AZO composite thin films with Cu thicknesses of 300 nm and 800 nm in the 350–800 nm wavelength range. Inset is the visual effect of optical transparency for polished CuM/AZO composite thin films on the PET substrates

transmittance is calculated to be 87.5% in the visible range of wavelengths (380–780 nm) for the single-layer AZO thin films grown on PET substrates. After combining with the 300 nm thick CuM, the average optical transmittance of the flexible composite thin films decreases slightly to 86.1%. The effect of the existence of CuM on the transmittance is very weak due to the large space between the Cu metallic meshes. When the thickness of CuM increases from 300 to 800 nm, only a marginal decrease in the average optical transmittance in the visible range of wavelengths is observed, which can be attributed to the nonrectangular shape of the photoresist trench and the over deposition of the metal copper.

Figure 3 shows the sheet resistance and resistivity of the single-layer AZO thin films and the CuM/AZO composite thin films with Cu thicknesses of 300 and 800 nm. In this paper, the thickness of composite thin films is the sum of the thicknesses of CuM and AZO. For the 300 nm thick single-layer AZO thin films on PET substrates in this study, the sheet resistance and resistivity are $9.32 \times 10^{-3} \Omega\text{-cm}$ and $318.2 \Omega/\text{sq.}$, respectively. After combined with CuM, the sheet resistance decreases drastically from $318.2 \Omega/\text{sq.}$ for the single-layer AZO thin films to $3.7 \Omega/\text{sq.}$ for the CuM/AZO composite thin films at 300 nm of Cu thickness. Correspondingly, the resistivity, like the sheet resistance also decreases drastically from 9.32×10^{-3} to $2.32 \times 10^{-4} \Omega\text{-cm}$. As further increasing the thickness of CuM to 800 nm, the sheet resistance and resistivity are further reduced to $1.9 \Omega/\text{sq.}$ and $1.89 \times 10^{-4} \Omega\text{-cm}$, respectively. The total resistance of CuM/AZO composite thin films can be assumed as a result of the parallel combination of the two individual layers (as seen in insert of

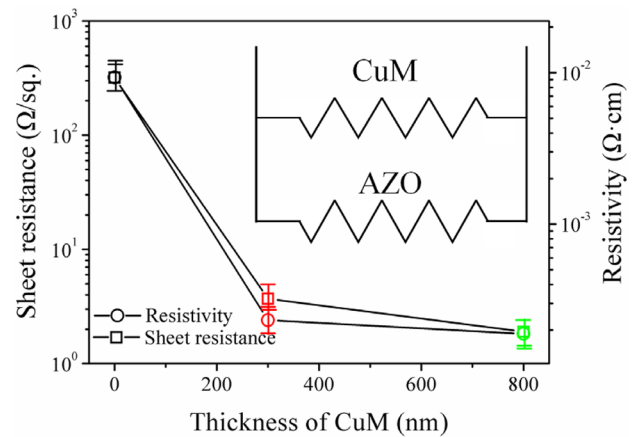


Fig. 3 Sheet resistance and resistivity of the single-layer AZO thin films and the CuM/AZO composite thin films with Cu thicknesses of 300 and 800 nm. Inset shows the electrical schematic of the CuM/AZO composite thin films

Fig. 3). The measured sheet resistance of the whole structure can be expressed as a function of the resistance of the single layers coupled in parallel:

$$R_{\text{Sq}} = \left(\frac{d_{\text{CuM}}}{\rho_{\text{CuM}}} + \frac{d_{\text{AZO}}}{\rho_{\text{AZO}}} \right)^{-1} \quad (2)$$

where, R_{Sq} is the sheet resistance of the CuM/AZO composite thin films, d_{CuM} is the thickness of the CuM, ρ_{CuM} is the resistivity of CuM, d_{AZO} is the thickness of AZO layers, and ρ_{AZO} is the resistivity of AZO layers. The resistance of the AZO layers in CuM/AZO composite thin films has been assumed to be constant in Eq. (2). The metallic Cu has excellent electrical conductivity, and the resistivity of the CuM is much lower than that of the AZO thin films. Therefore, the total resistance of CuM/AZO composite thin films mainly depends on resistivity of CuM, and the composite thin films have a much lower resistance than the single-layer AZO thin films of the same dimensions.

In order to evaluate the electrical properties of CuM/AZO composite thin films better, the Hall mobility of carrier concentration of composite thin films with different CuM thicknesses are investigated. The electrical conductivity can be determined by the concentration and Hall mobility of the carrier concentration, and explained using the following basic relation [40]:

$$\rho = \frac{1}{ne\mu} \quad (3)$$

where, ρ is the resistivity of samples, e is the charge of the carrier, n is the carrier concentration, and μ is the Hall mobility. From this equation, we can see that the resistivity is inversely proportional to the Hall mobility and carrier

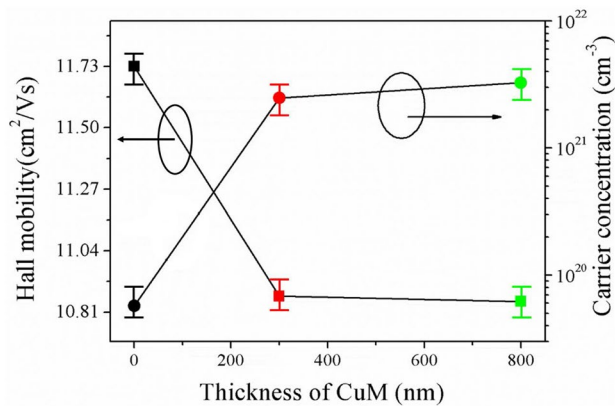


Fig. 4 Hall mobility and carrier concentration of the single-layer AZO thin films and the CuM/AZO composite thin films with CuM thicknesses of 300 and 800 nm

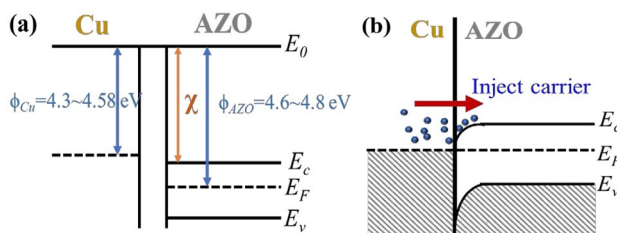


Fig. 5 Schematic energy band diagrams of AZO and CuM: **a** before contact and **b** after contact

concentration, which are closely related to the thin-film structure. Figure 4 shows the Hall mobility and carrier concentration of the single-layer AZO thin films and the CuM/AZO composite thin films with CuM thicknesses of 300 and 800 nm. The Hall mobility of the single AZO thin films is $11.73 \text{ cm}^2/\text{Vs}$. For the CuM/AZO composite thin films with Cu thickness of 300 nm, the Hall mobility slightly reduces to $10.87 \text{ cm}^2/\text{Vs}$, and the reduction in Hall mobility can be ascribed to the surface scattering at the AZO/CuM interfaces. With the thickness of CuM increasing to 800 nm, the Hall mobility almost remains constant, because there is no change in the interfacial area for AZO/CuM contact. As shown in Fig. 4, the plot indicates that the carrier concentration depends strongly on the thickness of CuM. The carrier concentration of the CuM/AZO composite thin films with the 300 nm thick CuM has increased by about two orders of magnitude compared to the single-layer AZO thin films. The carrier concentration of the CuM/AZO composite thin films has increased from 2.48×10^{21} to $3.27 \times 10^{21} \text{ cm}^{-3}$ with the increase of CuM thickness from 300 to 800 nm. Hence, metallic conduction is dominant in the CuM/AZO composite thin films.

Figure 5 shows schematic diagrams of the energy band structures that would be expected before and after AZO and metallic CuM are brought into contact, respectively. An analysis of the CuM/AZO composite thin films shows that the work function of AZO ($\phi_{\text{AZO}} = 4.6 - 4.8 \text{ eV}$) [41] is higher than that of Cu ($\phi_{\text{Cu}} = 4.3 - 4.58 \text{ eV}$) [42], resulting in the ohmic contact formation between AZO layer and CuM. After the CuM contacting with the AZO thin films, a great deal of electrons from the CuM inject straight into the AZO layer because of the difference of work functions between Cu and AZO, resulting in the accumulation of numerous electrons in a very small region near the interface. Due to the transfer of electrons, both the valence and conduction bands of AZO are curved downward. When a thermodynamic equilibrium is received, the Fermi level crosses the interface in a straight line at this moment, as shown in Fig. 5b. The barrier between CuM and AZO interfaces disappears at this time, and a great deal of electrons in the CuM flow into AZO thin films. As a consequence, the CuM/AZO composite thin films exhibit a very high carrier concentration. As we can see from Fig. 5, the carrier concentrations are observed to slightly increase with the increase of the thickness of CuM. The carrier concentration can be evaluated using the following equation:

$$n = \frac{N}{sd} \quad (4)$$

with

$$N = N_{\text{AZO}} + N_{\text{CuM}} \quad (5)$$

$$d = d_{\text{AZO}} + d_{\text{CuM}} \quad (6)$$

where N is the total number of carriers in the CuM/AZO composite thin films, N_{AZO} is the total number of carriers in the AZO layer, and N_{CuM} is the total number of carriers in the CuM layer. S is the surface area of the composite thin films. d , d_{AZO} and d_{CuM} are the thicknesses of the composite thin films, AZO and CuM layers, respectively. Since the total number of carriers of the CuM layer is much higher than that of the AZO layer, a simpler relation can be used:

$$n \cong \frac{N_{\text{CuM}}}{d_{\text{AZO}} + d_{\text{CuM}}} \quad (7)$$

Then, substituting $d_{\text{AZO}} = 300 \text{ nm}$ into Eq. (7), the formula can be rewritten as

$$\frac{n}{N_{\text{CuM}}} = \frac{1}{300 + d_{\text{CuM}}} \quad (8)$$

It can be clearly seen from Eq. (8) that the carrier concentration increases with the increase of the CuM thickness.

In various applications of transparent conductive thin films, both the optical transmittance and the electrical conduction are very important. Ideally, both the optical

transmittance and the electrical conduction should be as large as possible. However, their interrelation excludes the simultaneous achievement of the maximum transmittance and conduction in most cases. The figure of merit (FOM) φ_{TC} of the transparent conductive thin films can be defined as follows [43]:

$$\varphi_{TC} = \frac{T_{av}^{10}}{R_{sh}} \quad (9)$$

where, T_{av} is the average transmittance in visible light spectrum (considering the application of the thin films to solar cells and OLED, we use the average transmittance) and R_{sh} is the sheet resistance. The figures of merit can be calculated to be 0.08×10^{-2} , 6.05×10^{-2} and $11.4 \times 10^{-2} \Omega^{-1}$ for the single-layer AZO thin films and the CuM/AZO composite thin films with Cu thicknesses of 300 and 800 nm, respectively. Specifically, the CuM/AZO composite thin films with Cu thickness of 800 nm shows the highest FOM value. However, for the CuM/AZO composite thin films with thicker CuM thickness (above 800 nm), the CuM is easy to fall off during the lift-off process. Therefore, the thickness of CuM is controlled within 800 nm.

In order to have a well-defined physical meaning and gain further insight into how metal thickness affects the overall performance of the CuM/AZO composite thin films, another common *FoM* (F) is also used to better evaluate the optimal trade-off between the optical and electronic properties. F is more useful in comparing transparent conducting thin films [44]. The higher value of F indicates a more excellent performance of the thin film. The F value, namely, the ratio of electrical conductance to optical conductance (σ_{dc}/σ_{opt}), can be calculated via using the following widely accepted expression [44]:

$$\frac{\sigma_{dc}}{\sigma_{opt}} = \frac{Z_0}{2R_{sh}} \frac{\sqrt{T_{av}}}{1 - \sqrt{T_{av}}} \quad (10)$$

$$F = \frac{\sigma_{dc}}{\sigma_{opt}} \quad (11)$$

where σ_{dc} is the DC conductivity of the thin films, σ_{opt} is the optical conductivity at wavelength of λ nm, Z_0 is the impedance of free space (377Ω) and R_{sh} is the sheet resistance. It is worth noting that in our estimates we considered T_{av} as the average value over the visible wavelength region (380–780 nm). The F value of the single-layer AZO thin films on PET substrate is about 8.57. For the CuM/AZO composite thin films with Cu thicknesses of 300 and 800 nm, the F values are 655.67 and 1246.62, respectively, indicating their lower sheet resistance at the same optical transmission. Our flexible CuM/AZO composite thin films reveal a

F value of 1246.62 at 85.8% transmittance, which is higher than those of the commercial ITO on PET (100~150) [45, 46], carbon nanotube (31~64) [47, 48], graphene (~48) [49] and silver nanowire (100~350) [50, 51], copper nanowire (25~66) [52, 53] and hybrid transparent conductive thin films (10~200) [24–28, 54–57]. These data clearly indicate that the flexible CuM/AZO composite thin films boast superior overall performance compared with most other transparent conducting thin films.

In order to evaluate the flexibility of composite thin films under stress, the sheet resistance and average optical transmittance of both the single-layer AZO thin films and the CuM/AZO composite thin films are measured at a bending radius of $r=2$ mm (Fig. 6a, left). Figure 6a (right) shows a photograph of the CuM/AZO composite thin films on a PET substrate, demonstrating its flexibility and transparency. The sheet resistance variations obtained during the repetitive bending is represented by the $R_{sh}(b)/R_{sh}(0)$ ratio, where $R_{sh}(0)$ is the initial sheet resistance and $R_{sh}(b)$ is the sheet resistance measured when flattened after a certain number of bending cycles.

For choosing the appropriate bending radius, bending tests of CuM/AZO composite thin films with various bending radii ($r=1$ –15 mm) are carried out. For comparison, AZO coated on the PET film is used as a reference specimen. Results of these bending tests are given in Fig. 6b. From Fig. 6b we can see that the resistance of the bent CuM/AZO composite thin films doesn't change until it is bent to a bending radius of 1.5 mm. However, the reference AZO film shows an abruptly increased resistance change at a bending radius of 14 mm due to the rapid crack formation and propagation. This is the reason why $r=2$ mm has been chosen as the bending radius.

The sheet resistances of the single-layer AZO thin films and the CuM/AZO composite thin films after cyclic bendings, with bending radius of 2 mm, are shown in Fig. 6c. The initial $R_{sh}(b)/R_{sh}(0)$ ratios of the single-layer AZO thin films and the CuM/AZO composite thin films are all 1. Within less than 7 bending cycles, the $R_{sh}(b)/R_{sh}(0)$ ratio of the single-layer AZO thin films increases linearly to 12. On the other hand, the CuM/AZO composite thin films maintain a nearly similar resistance even after 500 bending cycles, indicating the excellent flexibility of the flexible CuM/AZO composite thin films. And this mechanical stability strengthens the merit of the CuM/AZO composite thin films with low resistance and high transparency, which are comparable to ITO. The average optical transmittances of the CuM/AZO composite and the single-layer AZO thin films versus the number of the bending cycles are also shown in Fig. 6c. From Fig. 6c we can see that, for all the thin-film samples, the optical transmittances decrease slightly within less than 5 bending cycles, and the values remain unchanged with further increasing the

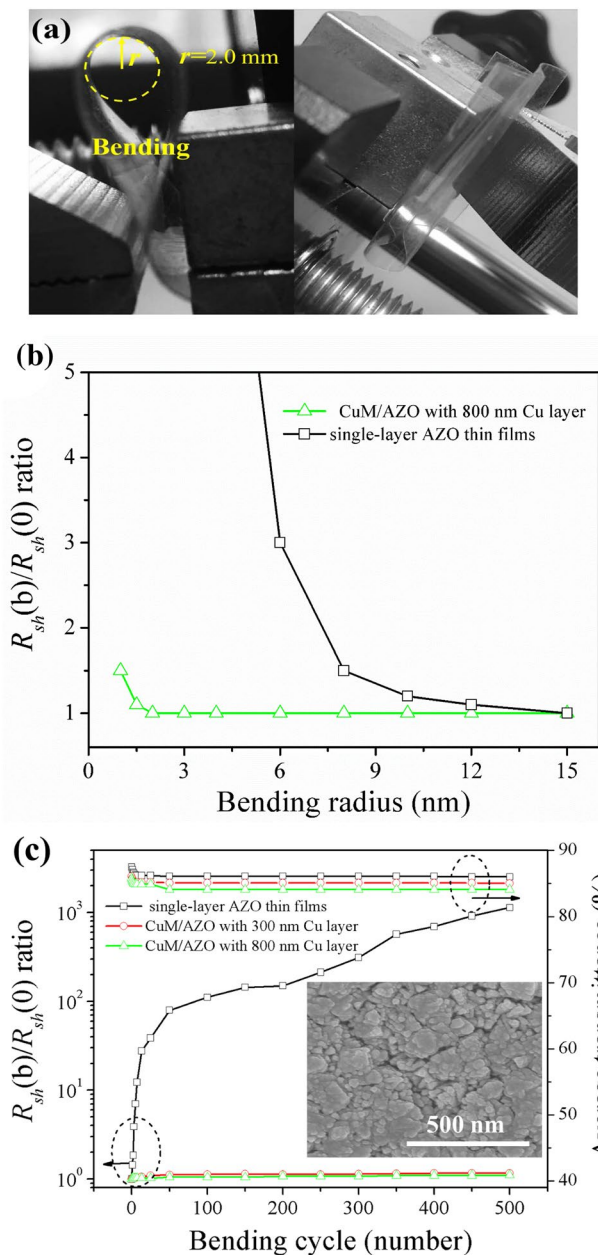


Fig. 6 **a** The bending and transpance photograph of the CuM/AZO composite thin films on a PET substrate; **b** Bending tests of CuM/AZO and AZO on a PET film with varying bending radius; **c** Sheet resistance and average optical transmittance after cyclic bendings. Insert shows the FE-SEM morphology of AZO films after 10 bending cycles

bending times. The reduction in the transmittance can be owing to the craze of AZO layer. After cyclic bendings, a lot of cracks are developed in the AZO layer due to the strain mismatch between the AZO and PET during the bending process (as shown in the inset of Fig. 6c). The cracks will scatter visible photons leading to the decrease of transmittance.

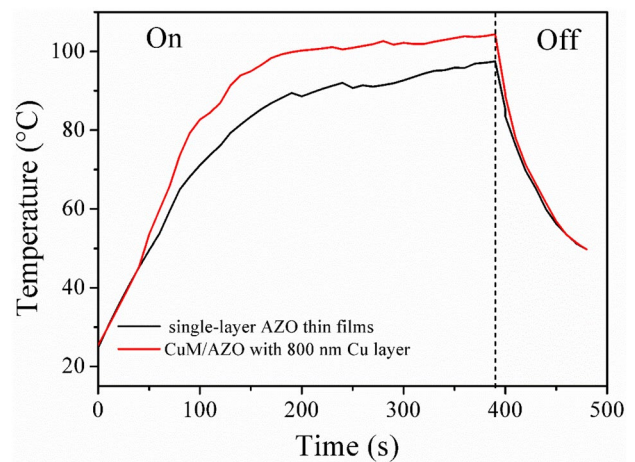


Fig. 7 Plots of temperature versus time for CuM/AZO and AZO transparent heater

To further show the credibility of their high performance, the application of the CuM/AZO composite thin films in optically transparent heater has been chosen as the example for illustration. For comparison, AZO (the single-layer AZO thin films) transparent heater is used as a reference specimen. The CuM/AZO transparent heater, with the CuM/AZO composite thin films (with Cu thickness of 800 nm) and two narrow silver paste lines along edges as contacts, has a resistance of $R_{sh} \approx 2 \Omega/\text{sq.}$, and it is subjected to voltage pulse of 1.5 V. Plots of temperature versus time for the CuM/AZO and AZO transparent heaters are shown in Fig. 7. From Fig. 7 it can be observed that for the CuM/AZO transparent heater the maximum temperature, $\sim 105^\circ\text{C}$, is obtained at the voltage of 1.5 V. However, for the AZO transparent heater the maximum temperature (95°C) is obtained at the voltage of 8.0 V. Apparently, the CuM/AZO transparent heater shows the lower drive voltage, which further indicates the high performance of the CuM/AZO thin films in the practical applications.

4 Conclusions

In summary, the flexible CuM/AZO composite thin films are successfully fabricated on PET substrates via combining the UV-lithography and the magnetron sputtering technologies. By increasing the thickness of CuM, a typical composite thin films with optical transmittance of 85.8%, sheet resistance of $1.9 \Omega/\text{sq.}$, resistivity of $1.89 \times 10^{-4} \Omega \cdot \text{cm}$ and figure of merit of 1247 are obtained. In the presence of CuM, the composite thin films show both improved flexibility and conductivity compared with the single-layer AZO thin films, which are beneficial for their applications in flexible electronic devices. In summary, owing to their outstanding performance, the

flexible CuM/AZO composite thin films demonstrate the potential for applications in high-performance flexible electronics and photovoltaic devices etc.

Acknowledgements This work was supported by the Natural Science Foundation of Tianjin City (Grant No. 18JCQNJC01300), National Natural Science Foundation of China (Grant Nos. 61701338 and 11502162), Foundation (B) for Peiyang Scholar-Young Core Faculty of Tianjin University (Grant No. 2018XRG-0020), and Scientific Research Foundation for High-Level Talents (Innovative Team) of Dongguan University of Technology (Grant No. KCYCXPT2017003).

References

- C. Lohaus, C. Steinert, G. Deyu, J. Brötz, W. Jaegermann, A. Klein, Enhancing electrical conductivity of room temperature deposited Sn-doped In_2O_3 thin films by hematite seed layers. *Appl. Phys. Lett.* **112**, 152105 (2018)
- B.B. Sahu, W. Long, J.G. Han, Highly conductive flexible ultra thin ITO nanoclusters prepared by 3-D confined magnetron sputtering at a low temperature. *Scr. Mater.* **149**, 98–102 (2018)
- K.P. Sibin, N. Swain, P. Chowdhury, A. Dey, N. Sridhara, H.D. Shashikala, A.K. Sharma, H.C. Barshili, Optical and electrical properties of ITO thin films sputtered on flexible FEP substrate as passive thermal control system for space applications. *Sol. Energy Mater. Sol. Cells* **145**, 314–322 (2016)
- H. Koseoglu, F. Turkoglu, M. Kurt, M.D. Yaman, F.G. Akca, G. Aygun, L. Ozyuzer, Improvement of optical and electrical properties of ITO thin films by electro-annealing. *Vacuum* **120**, 8–13 (2015)
- S.H. Park, S.M. Lee, E.H. Ko, T.H. Kim, Y.C. Nah, S.J. Lee, J.H. Lee, H.K. Kim, Roll-to-Roll sputtered ITO/Cu/ITO multilayer electrode for flexible, transparent thin film heaters and electrochromic applications. *Sci. Rep.* **6**, 33868 (2016)
- J. Gwamuri, A. Vora, J. Mayandi, D.Ö. Güney, P.L. Bergstrom, J.M. Pearce, A new method of preparing highly conductive ultra-thin indium tin oxide for plasmonic-enhanced thin film solar photovoltaic devices. *Sol. Energy Mater. Sol. Cells* **149**, 250–257 (2016)
- S. Naghdi, K. Rhee, D. Hui, S. Park, A review of conductive metal nanomaterials as conductive, transparent, and flexible coatings, thin films, and conductive fillers: different deposition methods and applications. *Coatings* **8**, 278 (2018)
- C.F. Guo, Z. Ren, Flexible transparent conductors based on metal nanowire networks. *Mater. Today* **18**, 143–154 (2015)
- N.T. Son, J.S. Noh, S. Park, Role of ZnO thin film in the vertically aligned growth of ZnO nanorods by chemical bath deposition. *Appl. Surf. Sci.* **379**, 440–445 (2016)
- J. Kennedy, P.P. Murmu, J. Leveneur, A. Markwitz, J. Futter, Controlling preferred orientation and electrical conductivity of zinc oxide thin films by post growth annealing treatment. *Appl. Surf. Sci.* **367**, 52–58 (2016)
- L. Wen, M. Kumar, B.B. Sahu, S.B. Jin, C. Sawangrat, K. Leksakul, J.G. Han, Advantage of dual-confined plasmas over conventional and facing-target plasmas for improving transparent-conductive properties in Al doped ZnO thin films. *Surf. Coat. Technol.* **284**, 85–89 (2015)
- Y. Li, R. Yao, H. Wang, X. Wu, J. Wu, X. Wu, W. Qin, Enhanced performance in Al-doped ZnO based transparent flexible transparent thin-film transistors due to oxygen vacancy in ZnO film with Zn–Al–O interfaces fabricated by atomic layer deposition. *ACS Appl. Mater. Interfaces* **9**, 11711–11720 (2017)
- J. Yang, Y. Jiang, L. Li, M. Gao, Structural, morphological, optical and electrical properties of Ga-doped ZnO transparent conducting thin films. *Appl. Surf. Sci.* **421**, 446–452 (2017)
- R.H. Horng, S.L. Ou, C.Y. Huang, P. Ravadgar, C.I. Wu, Effects of Ga concentration and rapid thermal annealing on the structural, optoelectronic and photoluminescence properties of Ga-doped ZnO thin films. *Thin Solid Films* **605**, 30–36 (2016)
- M. Wang, L. Jiang, Y. Wang, E.J. Kim, S.H. Hahn, Growth mechanism of preferred crystallite orientation in transparent conducting ZnO: in thin films. *J. Am. Ceram. Soc.* **98**, 3022–3028 (2015)
- C.Y. Tsay, H.C. Cheng, Y.T. Tung, W.H. Tuan, C.K. Lin, Effect of Sn-doped on microstructural and optical properties of ZnO thin films deposited by sol–gel method. *Thin Solid Films* **517**, 1032–1036 (2008)
- M. Wu, S. Yu, L. He, G. Zhang, D. Ling, W. Zhang, Influence of oxygen pressure on the structural, electrical and optical properties of Nb-doped ZnO thin films prepared by pulsed laser deposition. *Appl. Surf. Sci.* **292**, 219–224 (2014)
- M. Wu, S. Yu, G. Chen, L. He, L. Yang, W. Zhang, Structural, optical, and electrical properties of Mo-doped ZnO thin films prepared by magnetron sputtering. *Appl. Surf. Sci.* **324**, 791–796 (2015)
- S. Yu, B. Zhu, H. Zheng, L. Li, S. Chen, M. Lei, Effect of oxygen pressure performance of PZO thin films deposited by pulsed laser deposition at low temperature. *J. Alloys Compd.* **727**, 1273–1279 (2017)
- S. Yu, W. Zhang, L. Li, H. Dong, D. Xu, Y. Jin, Structural, electrical, photoluminescence and optical properties of n-type conducting, phosphorus-doped ZnO thin films prepared by pulsed laser deposition. *Appl. Surf. Sci.* **298**, 44–49 (2014)
- S. Fernandez, F.B. Naranjo, Optimization of aluminum-doped zinc oxide films deposited at low temperature by radio-frequency sputtering on flexible substrates for solar cell applications. *Sol. Energy Mater. Sol. Cells* **94**, 157–163 (2010)
- Y. Xia, P. Wang, G. He, M. Zhang, S. Shi, Y. Liu, Z. Sun, Microstructure, optoelectrical and pre-strain dependent electrical properties of AZO films on flexible glass substrates for flexible electronics. *Surf. Coat. Technol.* **320**, 34–38 (2017)
- H.R. Choi, S.K. Eswaran, S.M. Lee, Y.S. Cho, Enhanced fracture resistance of flexible ZnO: Al thin films in situ sputtered on bent polymer substrates. *ACS Appl. Mater. Interfaces* **7**, 17569–17572 (2015)
- G. Torrisi, I. Crupi, S. Mirabella, A. Terrasi, Robustness and electrical reliability of AZO/Ag/AZO thin film after bending stress. *Sol. Energy Mater. Sol. Cells* **165**, 88–93 (2017)
- S. Yu, Y. Liu, H. Zheng, L. Li, Y. Sun, Improved performance of transparent-conducting AZO/Cu/AZO multilayer thin films by inserting a metal Ti layer for flexible electronics. *Opt. Lett.* **42**, 3020–3023 (2017)
- H. Zhou, J. Xie, M. Mai, J. Wang, X. Shen, S. Wang, L. Zhang, K. Kisslinger, H.Q. Wang, J. Zhang, Y. Li, J. Deng, S. Ke, X. Zeng, High-quality AZO/Au/AZO sandwich film with ultralow optical loss and resistivity for transparent flexible electrodes. *ACS Appl. Mater. Interfaces* **10**, 16160–16168 (2018)
- T.C. Lin, W.C. Huang, F.C. Tsai, The structural and electro-optical characteristics of AZO/Cr: Cu/AZO transparent conductive film. *Thin Solid Films* **589**, 446–450 (2015)
- S. Yu, L. Zhao, R. Liu, C. Zhang, H. Zheng, Y. Sun, L. Li, Performance enhancement of Cu-based AZO multilayer thin films via graphene fence engineering for organic solar cells. *Sol. Energy Mater. Sol. Cells* **183**, 66–72 (2018)
- K. Ellmer, Past achievements and future challenges in the development of optically transparent electrodes. *Nat. Photonics* **6**, 809 (2012)
- W.K. Kim, S. Lee, D.H. Lee, I.H. Park, J.S. Bae, T.W. Lee, J.Y. Kim, J.H. Park, Y.C. Cho, C.R. Cho, S.Y. Jeong, Cu mesh for

- flexible transparent conductive electrodes. *Sci. Rep.* **5**, 10715 (2015)
31. Q. Huang, W. Shen, X. Fang, G. Chen, Y. Yang, J. Huang, R. Tan, W. Song, Highly thermostable, flexible, transparent, and conductive films on polyimide substrate with an AZO/AgNW/AZO structure. *ACS Appl. Mater. Interfaces* **7**, 4299–4305 (2015)
 32. B.J. Jeon, S. Lee, J.K. Lee, Adhesion characteristics of copper thin film deposited on PET substrate by electron cyclotron resonance-metal organic chemical vapor deposition. *Surf. Coat. Technol.* **202**, 1839–1846 (2008)
 33. V. Zardetto, T.M. Brown, A. Reale, A.D. Carlo, Substrates for flexible electronics: a practical investigation on the electrical, film flexibility, optical, temperature, and solvent resistance properties. *J. Polym. Sci. B* **49**, 638–648 (2011)
 34. K. Sakamoto, H. Kuwae, N. Kobayashi, A. Nobori, S. Shoji, J. Mizuno, Highly flexible transparent electrodes based on mesh-patterned rigid indium tin oxide. *Sci. Rep.* **8**, 2825 (2018)
 35. N. Joshi, V. Saxena, A. Singh, S.P. Koiry, A.K. Debnath, M.M. Chehimi, D.K. Aswal, S.K. Gupta, Flexible H₂S sensor based on gold modified polycarbazole films. *Sens. Actuators B* **200**, 227–234 (2014)
 36. R.R. Zhao, M.S. Yu, G.C. Wang, W. Liu, T.L. Chen, Ultra-flexible and robust transparent electrodes by embedding silver nanowires into polyimide matrix. *AIP Adv.* **8**, 065013 (2018)
 37. D. Foti, Use of recycled waste pet bottles fibers for the reinforcement of concrete. *Compos. Struct.* **96**, 396–404 (2013)
 38. B. Ollivier, S.J. Doney, S.J. Young, A. Matthews, Adhesion assessment of DLC films on PET using a simple tensile tester: comparison of different theories. *J. Adhes. Sci. Technol.* **9**, 769–784 (1995)
 39. W.G. Driscoll, W. Vaughan, *Handbook of Optics* (McGraw-Hill, New York, 1978)
 40. Y. Liu, Y.D. Qiao, G. Yang, Effect of thickness on the structural, morphological, electrical and optical properties of Nb plus Ta co-doped TiO₂ films deposited by RF sputtering. *Appl. Phys. A* **124**, 530 (2018)
 41. W.H. Kim, W.J. Maeng, M.K. Kim, H. Kim, Low pressure chemical vapor deposition of aluminum-doped zinc oxide for transparent conducting electrodes. *J. Electrochem. Soc.* **158**, D495–D499 (2011)
 42. C. Weichan, L. Shuhua, Z. Xiao, W. Xianhui, Y. Xiaohong, Effect of Mo addition on microstructure and vacuum arc characteristics of CuCr50 alloy. *Vacuum* **85**, 943–948 (2011)
 43. G. Haacke, New figure of merit for transparent conductors. *J. Appl. Phys.* **47**, 4086–4089 (1976)
 44. B. Han, K. Pei, Y. Huang, X. Zhang, Q. Rong, Q. Lin, Y. Guo, T. Sun, C. Guo, D. Carnahan, M. Giersig, Y. Wang, J. Gao, Z. Ren, K. Kempa, Uniform self-forming metallic network as a high-performance transparent conductive electrode. *Adv. Mater.* **26**, 873–877 (2014)
 45. H.J. Choi, S.G. Yoon, J.H. Lee, J.Y. Lee, Crystallized indium-tin oxide (ITO) thin films grown at low temperature onto flexible polymer substrates. *ECS J. Solid State Sci. Technol.* **1**, Q106–Q109 (2012)
 46. K.S. Tseng, Y.L. Lo, Effect of sputtering parameters on optical and electrical properties of ITO films on PET substrates. *Appl. Surf. Sci.* **285**, 157–166 (2013)
 47. F. Mirri, A.W.K. Ma, T.T. Hsu, N. Behabtu, S.L. Eichmann, C.C. Young, D.E. Tsentlovich, M. Pasquali, High-performance carbon nanotube transparent conductive films by scalable dip coating. *ACS Nano* **6**, 9737–9744 (2012)
 48. D.S. Hecht, A.M. Heintz, R. Lee, L. Hu, B. Moore, C. Cucksey, S. Risser, High conductivity transparent carbon nanotube films deposited from superacid. *Nanotechnology* **22**, 075201 (2011)
 49. C. Cai, F. Jia, A. Li, F. Huang, Z. Xu, L. Qiu, Y. Chen, G. Fei, M. Wang, Crackless transfer of large-area graphene films for superior-performance transparent electrodes. *Carbon* **98**, 457–462 (2016)
 50. Y. Zhang, J. Guo, D. Xu, Y. Sun, F. Yan, One-pot synthesis and purification of ultralong silver nanowires for flexible transparent conductive electrodes. *ACS Appl. Mater. Interfaces* **9**, 25465–25473 (2017)
 51. Y. Jiang, J. Xi, Z. Wu, H. Dong, Z. Zhao, B. Jiao, X. Hou, Highly transparent, conductive, flexible resin films embedded with silver nanowires. *Langmuir* **31**, 4950–4957 (2015)
 52. H.C. Chu, Y.C. Chang, Y. Lin, S.H. Chang, W.C. Chang, G.A. Li, H.Y. Tuan, Spray-deposited large-area copper nanowire transparent conductive electrodes and their uses for touch screen applications. *ACS Appl. Mater. Interfaces* **8**, 13009–13017 (2016)
 53. Z. Yin, S.K. Song, D.J. You, Y. Ko, S. Cho, J. Yoo, S.Y. Park, Y. Piao, S.T. Chang, Y.S. Kim, Novel synthesis, coating, and networking of curved copper nanowires for flexible transparent conductive electrodes. *Small* **11**, 4576–4583 (2015)
 54. C. Wu, T.W. Kim, F. Li, T. Guo, Wearable electricity generators fabricated utilizing transparent electronic textiles based on polyester/Ag nanowires/graphene core-shell nanocomposites. *ACS Nano* **10**, 6449–6457 (2016)
 55. Y. Ahn, Y. Jeong, D. Lee, Y. Lee, Copper nanowire-graphene core-shell nanostructure for highly stable transparent conducting electrodes. *ACS Nano* **9**, 3125–3133 (2015)
 56. Z. Zhu, T. Mankowski, K. Balakrishnan, A.S. Shikoh, F. Touati, M.A. Benammar, M. Mansuripur, C.M. Falco, Ultrahigh aspect ratio copper-nanowire-based hybrid transparent conductive electrodes with PEDOT: PSS and reduced graphene oxide exhibiting reduced surface roughness and improved stability. *ACS Appl. Mater. Interfaces* **7**, 16223–16230 (2015)
 57. J. Han, S. Yuan, L. Liu, X. Qiu, H. Gong, X. Yang, C. Li, Y. Hao, B. Cao, Fully indium-free flexible Ag nanowires/ZnO: F composite transparent conductive electrodes with high haze. *J. Mater. Chem. A* **3**, 5375–5384 (2015)

Publisher's Note Springer Nature remains neutral with regard to jurisdictional claims in published maps and institutional affiliations.